buildings

MDPI

Article

Cyclic Behavior of Rectangular Bridge Piers Subjected to the Coupling Effects of Chloride Corrosion and Bidirectional Loading

Wenting Yuan [1,2,*], Xinping Li [2], Xiaohang Pang [2], Chao Tian [2], Zelong Li [2], Peng Zhou [2] and Yuren Wang [2]

[1] Institute of Transportation, Inner Mongolia University, Hohhot 010070, China
[2] State Key Laboratory for Geomechanics & Deep Underground Engineering, School of Mechanics and Civil Engineering, China University of Mining and Technology, Xuzhou 221116, China
* Correspondence: 18704657392@163.com

Abstract: The degradation of seismic performance for RC bridge piers induced by chloride corrosion has previously been studied by treating the earthquake as a unilateral cyclic loading. Such studies do not consider the true response of the pier under the joint effect of corrosion damage and real multi-dimensional earthquake action. Thus, in the present study, the cyclic behavior of rectangular bridge piers subjected to the coupling effects of chloride corrosion and bidirectional loading was numerically investigated. First, the corrosion-induced deterioration of material mechanical properties is introduced. Second, the numerical model of two corroded piers is built and validated with the test results in the literature. Then, the time-dependent biaxial seismic performance of a rectangular bridge pier under the circular-shaped (CS) biaxial displacement pattern, square-shaped (SS) biaxial displacement pattern, uniaxial displacement in the X-direction (UX) pattern, and uniaxial displacement in the Y-direction (UY) pattern is analyzed using the validated model. The simulation results conclude that the trajectory of biaxial loading paths and corrosion levels significantly influence the peak force, deformation capacity, and dissipated energy of the piers. The biaxial loading path effect for the corrosive pier includes two stages with different biaxial force trajectory characteristics. Compared with the uncorroded pier, the corrosion level of 13.7% and biaxial loading induces up to a 40% reduction in strength and a 54% decrease in the residual ultimate displacement of the corroded pier. For the same corrosion degree, the dissipated energy under the SS biaxial displacement path is the largest among the four loading paths.

Keywords: bridge piers; corrosion; cyclic behavior; bidirectional loading; strength

check for updates

Citation: Yuan, W.; Li, X.; Pang, X.; Tian, C.; Li, Z.; Zhou, P.; Wang, Y. Cyclic Behavior of Rectangular Bridge Piers Subjected to the Coupling Effects of Chloride Corrosion and Bidirectional Loading. *Buildings* **2023**, *13*, 425. https://doi.org/10.3390/buildings13020425

Academic Editor: Oldrich Sucharda

Received: 12 December 2022
Revised: 25 January 2023
Accepted: 1 February 2023
Published: 3 February 2023

Copyright: © 2023 by the authors. Licensee MDPI, Basel, Switzerland. This article is an open access article distributed under the terms and conditions of the Creative Commons Attribution (CC BY) license (https://creativecommons.org/licenses/by/4.0/).

1. Introduction

Nowadays, large numbers of reinforced concrete (RC) bridges have been built around the world. These bridges inevitably suffer from steel corrosion, leading to mechanical properties degradation of steel and concrete [1,2], bonding strength degradation [3], and eventually continuous structural performance deterioration [4,5]. Different from continuous environmental corrosion, earthquake is an occasional but destructive natural hazard that threatens the service safety of bridges. Therefore, the corrosion effect needs to be considered during the seismic assessment of long-term serviced bridges.

As the key element of bridges, the corroded RC piers under simulated uniaxial seismic loading have attracted many scholars' attention. Yuan et al. [6] reported the seismic performance of RC columns considering the joint effect of rebar corrosion and axial loading protocols. Meda et al. [7] tested two full-scale RC columns under cyclic loading and found a 50% decrease in the ultimate deformation capacity of columns due to a 20% reinforcement corrosion degree. Li et al. [8] reported a quasi-static cyclic test of six RC columns and found that non-uniform corrosion led to an asymmetric phenomenon in the structural performance degradation in the positive and negative directions. Dai et al. [9]

conducted an experimental investigation on the cyclic behavior of corroded RC columns using electrochemical chloride extraction (ECE) and artificial climate environment (ACE) techniques. Guo et al. [10] and Yuan et al. [11] finished cyclic tests on coastal piers with non-uniform corrosion damage and highlighted the transfer mechanism of the plastic hinge of corroded piers. The plastic hinge transfer phenomenon caused by corrosion was also observed in the quasi-static tests of RC column specimens conducted by Zhou et al. [12] and Zhao et al. [13]. Experimental studies [14,15] showed that corroded RC columns had a smaller energy dissipation capacity and more obvious stiffness degradation phenomenon compared with those of the uncorroded columns. Based on the cyclic tests of Beam-Columns, Chinnasamy et al. [16] concluded that the load-carrying capacity of GFRP beam-columns can be significantly improved by replacing cement with high-volume fly ash engineered cementitious composites. Kashani et al. [17] developed a fiber-based element model considering the inelastic buckling of corroded longitudinal rebars to predict the seismic performance of RC piers. Cheng et al. [18] simulated the cyclic behavior of corroded piers with consideration of the strain penetration effect. Xu et al. [19] evaluated the seismic failure mode and bearing capacity of corroded RC columns with the aid of a machine learning-based approach. On the basis of numerical simulation, El-Joukhadar et al. [20] proposed a modified resistance envelope for corroded columns, which considered the stiffness, strength, and deformation capacity reduction due to corrosion. To investigate the time-dependent seismic fragility of RC bridges, studies [21,22] modelled the cyclic performance of pier columns considering the influence of both uniform corrosion and pitting corrosion on the mechanical properties of steel bars and concrete.

In reality, an earthquake has the property of randomness directionally and can be simplified as two-dimensional loads in the horizontal direction [23]. Considering this phenomenon, the behavior of the pier column under biaxial lateral seismic excitation was studied. Qiu et al. [24] explored the seismic performance of seven square RC columns via quasi-static tests with different biaxial loading paths and found that the coupling effect of biaxial load led to a decrease in strength and an increase in structural damage. Tsuno and Park [25] reported biaxial cyclic tests of five RC columns and found that the ductility and peak force of the uniaxially loaded column was larger than that of the biaxially loaded column. Jia et al. [26] investigated the biaxial seismic performance of self-centering precast bridge piers based on a quasi-static test with an oblique loading pattern. The results showed that the local damage and residual displacement of the pier were influenced by the loading direction. Rodrigues et al. [27] and Rodrigues et al. [28] analyzed the seismic performance of retrofitted columns and un-retrofitted RC columns through a great deal of biaxial cyclic tests. Besides experiments, the numerical method is another effective means of understanding the biaxial seismic behavior of columns. Based on simulation results, Li et al. [29] concluded that biaxial loading led to larger residual drift and more significant strength degradation of precast piers than that of the uniaxial loading condition. Through the numerical model, Shirmohammadi and Esmaeily [30] found that axial load level and bilateral loading patterns were two important factors of the biaxial cyclic responses for the RC columns. Al-Kaseasbeh and Mamaghani [31] built a finite element model of thin-walled steel stiffened square box columns in ABAQUS and simulated the structural behavior of columns under bi-directional cyclic loading.

From the above-mentioned studies, it can be concluded that corrosion weakens the seismic capacity of RC pier columns, and biaxial seismic excitations will make the structural performance deterioration even worse. Aimed at this problem, Zheng et al. [32] conducted biaxial cyclic experiments on ten corroded bridge columns under elliptical-shaped biaxial displacement paths. Test results showed that the stiffness, peak force, and ductility in the two orthogonal loading directions of piers dropped with the rise in corrosion. Yuan et al. [33] tested four corrosion variable bridge pier specimens under bilateral cyclic loading and found that the seismic performance of piers was significantly influenced by corrosion degree and rectangular-shaped biaxial displacement protocol. Studies [32,33] provided valuable findings about the biaxial seismic performance of corroded RC columns. However,

the corrosion conditions were few, and only one kind of biaxial displacement pattern was adopted in each study. The coupling effect of chloride corrosion and bidirectional loading on the biaxial seismic performance of long-term serviced bridge piers still needs to be investigated.

To deal with this problem, the seismic performance of RC bridge piers considering both biaxial loading path and corrosion degree is studied through numerical simulation. In Section 2, the degradation of material mechanical properties for RC components is briefly introduced. In Section 3, a numerical model of the corroded pier is built and verified with the experimental results in the literature. Employing the validated simulation method, an illustrative example of a rectangular bridge pier is presented in Section 4, and the time-variant bidirectional seismic behavior of corroded piers is analyzed. Finally, the main conclusions are summarized in Section 5.

2. Degradation of Material Properties

For reinforced concrete bridge piers with long-term service periods, chloride-induced reinforcement corrosion is one of the main factors that threaten structural durability. Once corrosion is initiated, the material's mechanical properties of reinforcing steel are deteriorated, leading to the degradation of mechanical behavior for the corroded pier over time.

2.1. Time of Corrosion Initiation

Chloride ions in the corrosion environment penetrate through the concrete cover of the pier to the surface of the reinforcing steel. After the passivation film dissolves and the chloride ions accumulate to a certain extent, chloride corrosion of the reinforcing steel is initiated. The corrosion initiation time, t_{ini}, can be predicted by a simple expression as [34].

$$t_{\mathrm{ini}} = \frac{c^2}{4D_{\mathrm{c}}}\left[erf^{-1}\left(\frac{C_0 - C_{cr}}{C_0}\right)\right]^{-2} \tag{1}$$

where *erf* is the error function, D_{c} is the chloride diffusion coefficient, C_{cr} is the critical chloride concentration, and C_0 is the equilibrium chloride concentration at the surface of the concrete cover. In reality, the parameters of the corrosion environment are random. The mean value of the random variables, D_{c}, C_{cr}, and C_0, from studies [35–37] are used in Formula (1) to determine the corrosion initiation time.

2.2. Deterioration of Reinforcing Steel

Once corrosion starts, the cross-sectional area of the reinforcement reduces. Considering the adverse effects of pit corrosion, the corroded cross-sectional area, $A_{\mathrm{pit}}(t)$, of the reinforcing bar can be expressed as [38].

$$A_{\mathrm{pit}}(t) = \begin{cases} A_1 + A_2, & p(t) \le \frac{\sqrt{2}}{2}d_0 \\ \frac{\pi d_0^2}{4} - A_1 + A_2, & \frac{\sqrt{2}}{2}d_0 \le p(t) \le d_0 \\ \frac{\pi d_0^2}{4}, & p(t) > d_0 \end{cases} \tag{2}$$

$$A_1 = \frac{1}{2} \times \left[2 \cdot \arcsin\left(\frac{2 \cdot p(t) \cdot \sqrt{1 - \left(\frac{p(t)}{d_0}\right)^2}}{d_0}\right) \cdot \left(\frac{d_0}{2}\right)^2 - 2 \cdot p(t) \cdot \sqrt{1 - \left(\frac{p(t)}{d_0}\right)^2} \cdot \left|\frac{d_0}{2} - \frac{p(t)^2}{d_0}\right|\right] \tag{3}$$

$$A_2 = \frac{1}{2} \times \left[2 \cdot \arcsin\left(\frac{2 \cdot p(t) \cdot \sqrt{1 - \left(\frac{p(t)}{d_0}\right)^2}}{2 \cdot p(t)}\right) \cdot p(t)^2 - 2 \cdot p(t) \cdot \sqrt{1 - \left(\frac{p(t)}{d_0}\right)^2} \cdot \frac{p(t)^2}{d_0}\right] \tag{4}$$

where d_0 is the diameter of the uncorroded reinforcing bar and $p(t)$ is the pitting depth of the corroded reinforcement at time, t, which can be quantified by Formula (5) [39].

$$p(t) = 0.0116 i_{\text{corr}}(t - t_{ini}) R_{\text{pit}} \tag{5}$$

where R_{pit} is the amplification factor related to the pit corrosion and i_{corr} is the corrosion current density.

Accompanied by the section dimension decrease, the mechanical properties of reinforcing steel reduce, which can be expressed as Formulas (6) and (7) [40,41].

$$f_{\text{y}}(t) = [1 - 0.005 \cdot Q_{\text{corr}}(t)] \cdot f_{\text{y0}} \tag{6}$$

$$Q_{corr}(t) = (A_{\text{pit}}(t)/A_{s0}) \times 100 \tag{7}$$

where $Q_{\text{corr}}(t)$ is the mass loss ratio (corrosion level) of the corroded reinforcement with an initial cross-sectional area of A_{s0} and an initial yield strength of f_{y0}; $f_{\text{y}}(t)$ is the deteriorated yield stress of the corroded reinforcement.

2.3. Deterioration of Concrete

Corrosion leads to cracking of the concrete cover. The cracking of the concrete cover is a three-dimensional brittle fracture problem that can be characterized by the crack depth, crack width, and crack frequency [42]. The cracking of concrete further influences the corrosion process of reinforcement. As a result, there is a vicious circle of the mechanical performance of the cracked concrete cover. To simplify this complex mechanical behavior deterioration phenomenon, based on the existing studies [43,44], and considering that the mechanical behavior of the concrete cover can be neglected when the crack width reaches 1 mm, the following piecewise function is adopted to quantify the strength of the concrete cover:

$$f_{\text{c}}(t) = \begin{cases} \frac{f_{\text{c0}}}{1+K\varepsilon_1(w_{cr}(t))/\varepsilon_{\text{c0}}} & w_{cr}(t) < 1mm \\ 0 & w_{cr}(t) \geq 1mm \end{cases} \tag{8}$$

where f_{c0} is the compression strength of the pristine concrete and $\varepsilon_1(w_{cr}(t))$ is the mean value of the tensile strain for the cracked concrete, which is a function of corrosion-induced crack width $w_{\text{cr}}(t)$. $w_{\text{cr}}(t)$ can be calculated as [44].

$$w_{\text{cr}}(t) = k_{\text{w}}[\delta_{\text{s}}(t) - \delta_{\text{s0}}]A_{\text{s0}} \tag{9}$$

where δ_{s0} is the amount of steel damage that leads to cracking initiation and $\delta_{\text{s}}(t)$ is the reduction percentage of cross-sectional area for the steel. It should be noted that only corrosion-induced cracking is considered in Equation (9) of this study. When the fatigue crack, as mentioned in [45,46], is determined and incorporated into Equation (9), more complex concrete cracking phenomenon for the long term serviced bridge pier can be simulated.

Due to the corrosion of stirrups, the confinement effect is weakened. By calculating the yield stress and cross-sectional area of the corroded stirrups, the mechanical behavior of the deteriorated core concrete can be quantified using the Mander model [47].

3. Numerical Model of the Corroded Pier and Validation

This section presents the experimental validation of the numerical method in Section 2. First, the dimension and reinforcement details, and the material properties for reinforcement and concrete, and the corrosion conditions and loading protocols of bridge pier specimens is briefly introduced. Second, a fiber-based numerical model of the corroded pier specimens is built. Finally, the simulated and experimental cyclic curves of specimens are compared.

3.1. Description of Bridge Pier Specimens

Two corroded circular pier specimens, D130 and D150, subjected to unilateral cyclic loading [11] were selected to validate the numerical method. These two specimens had the same dimension and reinforcement details, as shown in Figure 1. Each specimen was reinforced by 10 ϕ 14 mm longitudinal rebars and ϕ 8 mm spirals. At the top and bottom region of the pier shaft with a height of 500 mm, the spacing of spirals was 70 mm. The corresponding value for the spirals in the remaining part of the pier shaft was 100 mm. The yield strength for spirals and longitudinal rebars were 291 and 356 MPa, respectively. The ultimate strength for spirals and longitudinal rebars were 455 and 517 MPa. The compression strength of concrete was 36.3 MPa. The thickness of the concrete cover was 20 mm. For Specimen D130, the average mass loss ratio, Q_{corr}, for spirals and longitudinal reinforcement was 51.66% and 28.52%, respectively. The corresponding value for Specimen D150 was 55.42% and 30.71%, respectively. Each pier specimen was tested under unilateral cyclic loading displacement. At first, the preloading displacement amplitudes of 2 mm and 4 mm were used, and each displacement was applied once. The subsequent displacement was repeated twice, and the corresponding displacement amplitude was increased as Δ_1 = 8 mm, $2\Delta_1$, $3\Delta_1$, . . . , until the pier failed. More details about the tests of the two specimens can be found in the above-mentioned reference.

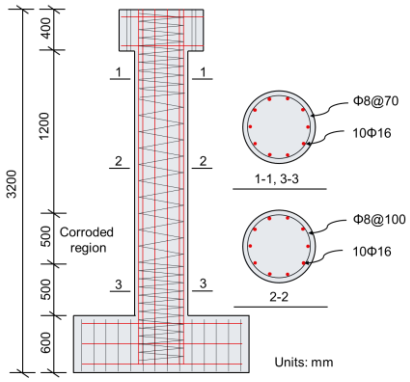


Figure 1. Dimension and reinforcement details of each specimen.

3.2. Numerical Modeling Details and Validation

Using the Opensees software package [48], the numerical model of each specimen was built and are presented in Figure 2. Each specimen was simulated by 5 nonlinear beam column fiber elements with 6 nodes. The cross-section of each element was discretized into rebar and concrete fibers. The stress–strain behavior of the rebar fibers was modeled by the constitutive models of Steel02. For concrete fibers whose tensile strength is fa smaller than their compression strength, they were modeled by the widely used constitutive models of Concrete01. For the corrosion damage region of each specimen, its deterioration of mechanical properties for rebar fibers with the reduced cross-sectional area and concrete fibers were simulated using the method of Section 2.

The experimental and computed cyclic curves of specimens D130 and D150 are compared in Figure 3. As shown in Figure 3, the numerical model does well in capturing the stiffness, peak force, and strength degradation behavior of specimens D130 and D150. The error in the peak strength of specimen D130 along the negative and positive directions was found to be 6.32% and 5.53%, respectively. The corresponding value for specimen D150 was 0.5% and 14.39%, respectively. Due to the non-uniform corrosion of reinforcement and discrepancy of concrete material, the pinch behavior of the two specimens and the asymmetrical phenomenon of cyclic loops (Specimen D150) are not well simulated. Overall, it is demonstrated that the developed numerical model can be extended to investigate the seismic behavior of rectangular RC bridge piers subjected to biaxial cyclic loadings and corrosion damage.

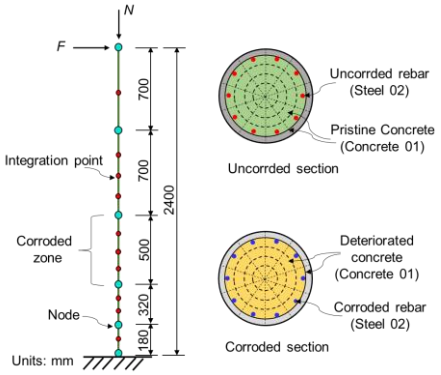


Figure 2. Fiber-based numerical model of each specimen.

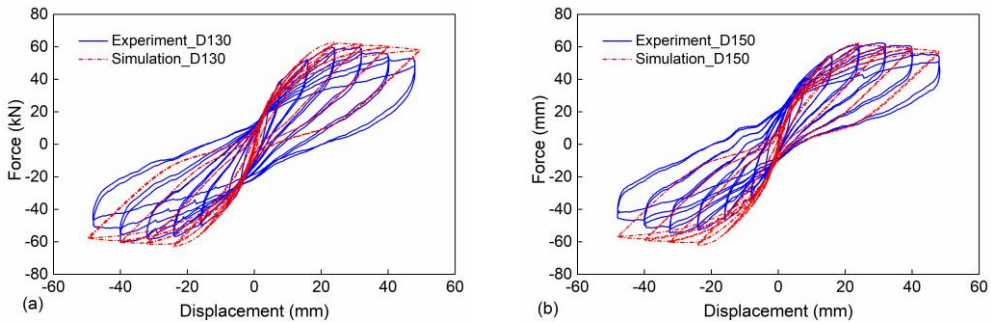


Figure 3. Experimental and numerical comparison: (**a**) Specimen D130; (**b**) Specimen D150.

4. Illustrative Example of the Rectangular Bridge Pier

4.1. Description of the Bridge Pier

A typical box-girder bridge with a single column bent in California [49] was selected for analysis in the present study. The pier column (see Figure 4) had a clear height of 7.43 m with a section dimension of 1829 mm × 1219 mm. The deck had a width of 9.78 m and a height of 1.74 m. In the bridge pier, there were 42 longitudinal steel elements with a diameter of 36 mm; 14 mm diameter rebar @ 100 mm was adopted for stirrups. Both stirrups and longitudinal rebars had an initial yield strength of 465 MPa. The concrete cover had a depth of 50.8 mm and a compression strength of 29.3 MPa. A mass of 790 tons was transferred from the superstructure to the pier top.

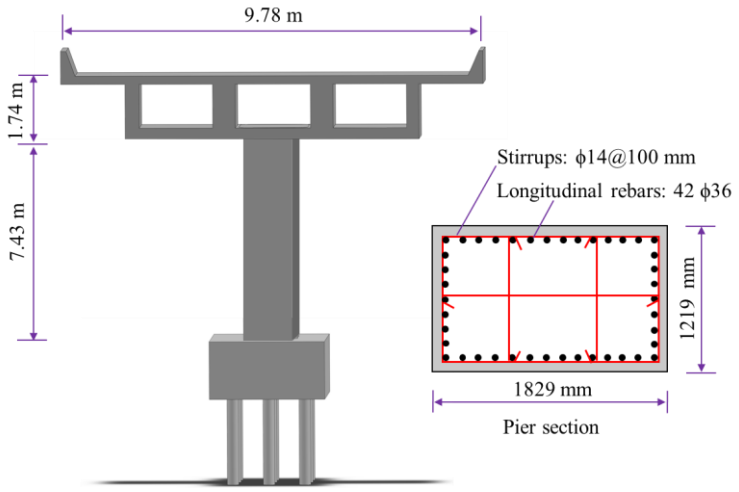


Figure 4. Details of the bridge pier.

The bridge pier was located in a chloride environment, and the corresponding corrosion parameters were adopted from existing studies [35–37]. The critical chloride con-

centration, C_{cr}, and the equilibrium chloride concentration, C_0, were taken as 0.9 kg/m^3 and 2.95 kg/m^3, respectively. The chloride diffusion coefficient, D_c, was 2 × 10^{-8} cm^2/s. Corrosion current density, i_{corr}, was taken as 3 μA/ cm^2. R_{pit} was assumed to be 6.

4.2. Deterioration of Material

Based on Formula (1), the corrosion initiation time for stirrups was calculated to be 22.8 years. The corresponding value for longitudinal reinforcement was 37.1 years, which is larger than that of the stirrups. Further, the time-dependent corrosion level and residual yield strength for longitudinal reinforcement and stirrups were obtained using Formulas (6) and (7), as shown in Figure 5. From Figure 5, it can be seen that the corrosion level of the stirrups increases with time after corrosion initiation. At 85 years, the corrosion level reaches 95.5%, and the stirrups are almost rusted off. The corresponding value for longitudinal reinforcement is 13.7%. During the time range of 0 to 85 years, the yield strength for stirrups and longitudinal reinforcement reduces from 465 MPa to 243 MPa and 433 MPa, respectively. For the concrete cover, its compression strength decreases from 29.3 MPa to 27.6 MPa and 22.9 MPa at 50 years and 55 years, respectively. When the crack width reaches 1 mm after 55 years, the compression strength of the deteriorated concrete cover drops to zero.

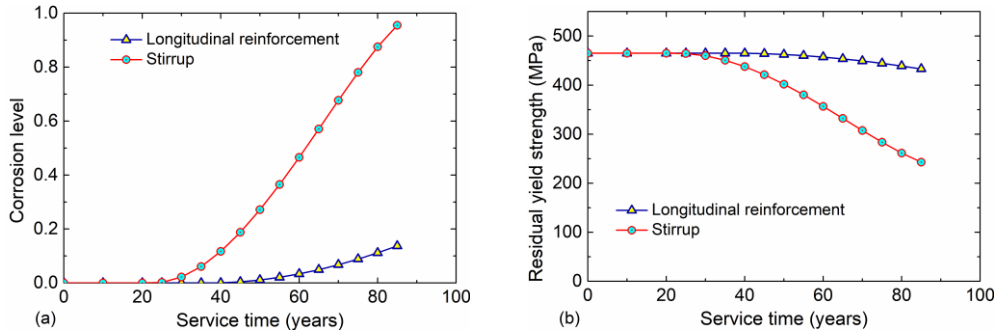


Figure 5. Time-variant performance of steel rebars: (**a**) corrosion level; (**b**) residual yield strength.

4.3. Numerical Model and Biaxial Loading Protocols

Based on the time-dependent material deterioration model, the fiber-section model of the rectangular bridge pier was built, as shown in Figure 6. Each specimen was simulated by 3 nonlinear beam column fiber elements with 4 nodes. To investigate the biaxial seismic performance of corroded bridge piers, the loading protocols should be selected first. Considering that the circular-shaped (CS) and square-shaped (SS) biaxial loading displacement patterns were commonly used protocols [30,31], these two displacement patterns were adopted in the simulation. Furthermore, the uniaxial displacement pattern in the X-direction (UX) and the uniaxial displacement pattern in the Y-direction (UY) were also selected for comparison. The four biaxial loadings have different protocols, but the same displacement amplitudes, which begin with 18.75 mm (drift ratio of 0.25%), are multiplied. Each displacement amplitude was repeated twice. To apply biaxial loading displacement in Opensees software, the LoadPattern object was used for both the X- and Y-directions. Each plain load pattern is associated with a TimeSeries object and SP_Constraint objects. Each TimeSeries object contains the displacement data determined by the SS or CS displacement patterns described in Figure 6.

4.4. Hysteretic Curve

The hysteretic curve of the pier under the coupling effect of biaxial loading and corrosion for 0 to 85 years with a time interval of 5 years was obtained. Due to the space limitation, Figures 7–9 only show the cyclic curves at three different times. From Figure 7, it can be seen that the lateral force of the pristine pier increases with deformation and reaches a peak at the displacement of 112.5 mm. At this stage, the residual displacement

and damage of the pier are small. With a further increase in displacement, the lateral force drops compared with the peak force. When the pier is corroded at 55 and 85 years, the hysteretic performance obviously deteriorates, which is characterized by reduced strength and cyclic loop area. Figure 7 also shows that the strength, deformation capacity, and area of the hysteretic curve in the X-direction is smaller than that in the Y-direction for the same corrosion level. This can be attributed to the fact that the pier has a weak axis (X-direction) and a strong axis (Y-direction). From Figure 7, it can also be seen that the pinch behavior of the cyclic curve is reduced with the increase in corrosion level.

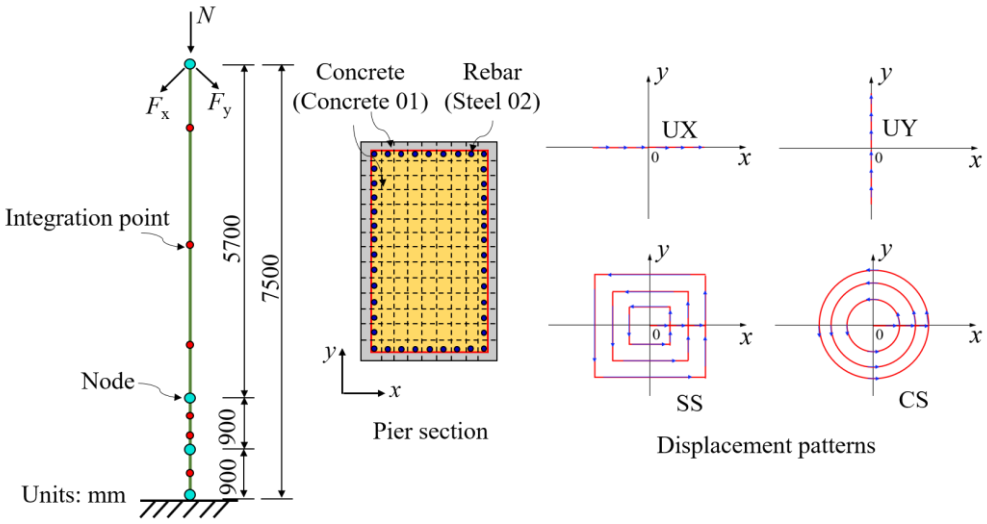


Figure 6. Numerical model of the bridge pier.

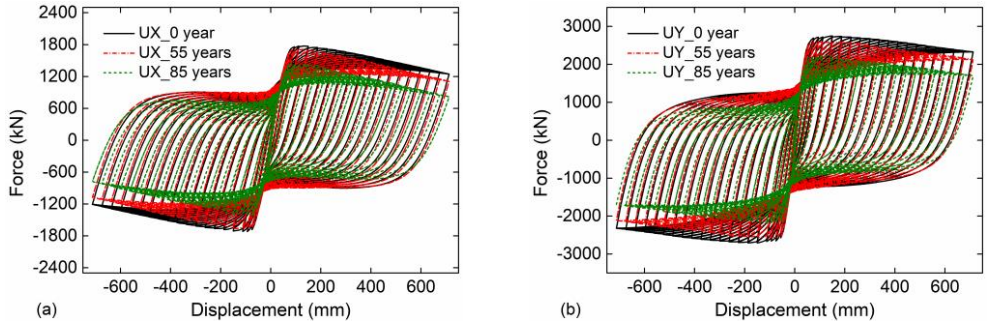


Figure 7. Cyclic curve for the UN path: (**a**) X-direction; (**b**) Y-direction.

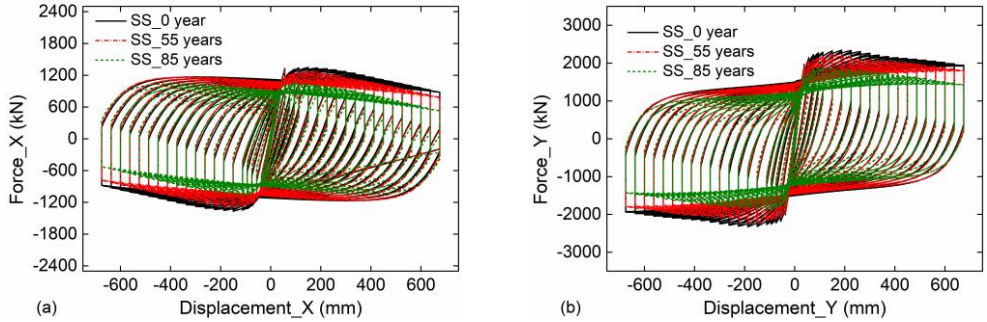


Figure 8. Cyclic curve for the SS path: (**a**) X-direction; (**b**) Y-direction.

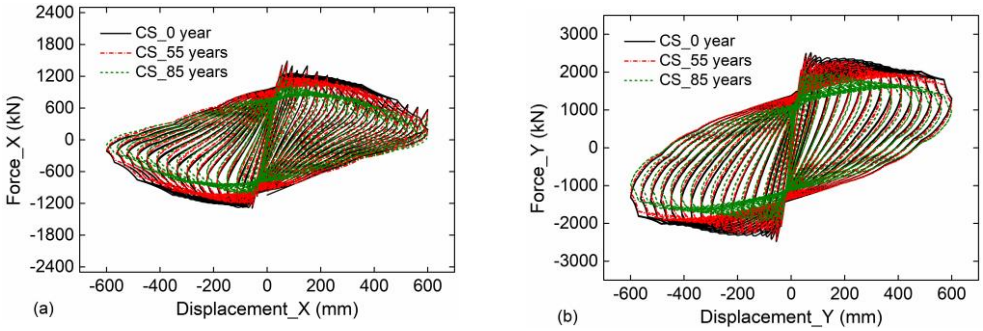


Figure 9. Cyclic curve for the CS path: (**a**) X-direction; (**b**) Y-direction.

Under the SS pattern, as shown in Figure 8, the cyclic response of the pier is different from that of the uniaxial loading path. When the displacement in one direction of the biaxially loaded pier is fixed, the displacement in the orthogonal direction increases, leading to a significant reduction of force. Due to this coupling effect, the force corresponding to each displacement level under the SS pattern is smaller than that of the uniaxial loading condition. Similar to the uniaxial loading condition, the cyclic performance for the pier under the SS pattern decreases with corrosion.

The hysteretic curve under the CS pattern is oval-shaped, as shown in Figure 9. The seismic performances of the pier in two orthogonal directions are both influenced by the strong coupling effect. As a result, for the same corrosion degree and displacement, the corresponding lateral force of the column subjected to the CS path is smaller than that of the uniaxial loading condition. Furthermore, it can be seen that the difference of peak force between the CS path and the SS path is not obvious.

From the above analysis, it can be concluded that biaxial seismic excitation and corrosion damage will significantly threaten the seismic safety of a pier designed with uniaxial loading.

4.5. Loading Path Effect

The loading path effect reflects the interaction of force in the two loading directions. To analyze this phenomenon, the biaxially loaded pier under 0 years and 85 years was selected as an instance. The relationship between the lateral force in the X-direction and the force in the Y-direction was picked out from the cyclic curves and is presented in Figures 10 and 11. In Figures 10 and 11, the biaxial force trajectory at 0 years (uncorroded condition) is represented by green solid lines. The biaxial force trajectory for the corroded piers at 85 years is represented by orange dash-dotted lines. As Figure 10 shows, the force trajectory is rectangular-shaped under the square-shaped displacement path for the first two displacement amplitudes (18.75 mm and 37.5 mm) of the pier. For the circular-shaped displacement protocol, the shape of the biaxial force trajectory is elliptical. In this displacement level, the pier under the SS path and the CS path is in the elastic stage, and the coupling effect can be ignored.

With the pier entering into the plastic stage, which corresponds to a displacement amplitude larger than 37.5 mm, the biaxial force trajectory overall torsions anti-clockwise compared with the elastic stage. This phenomenon indicates the significant coupling effect of the biaxial loading condition. Figures 10 and 11 also show that the trend of biaxial force trajectory for the uncorroded pier and corroded pier is similar under the same displacement protocol. Furthermore, the enclosed area of biaxial force is decreasing with the increase in time for the same displacement amplitude. This phenomenon means that corrosion induces biaxial strength deterioration. For the biaxially loaded pier at other service times, the same conclusions can be obtained as the condition of 0 years and 85 years. Due to space limitation and to avoid curve coverage, the biaxial force trajectory for other service times is not plotted in Figures 10 and 11.

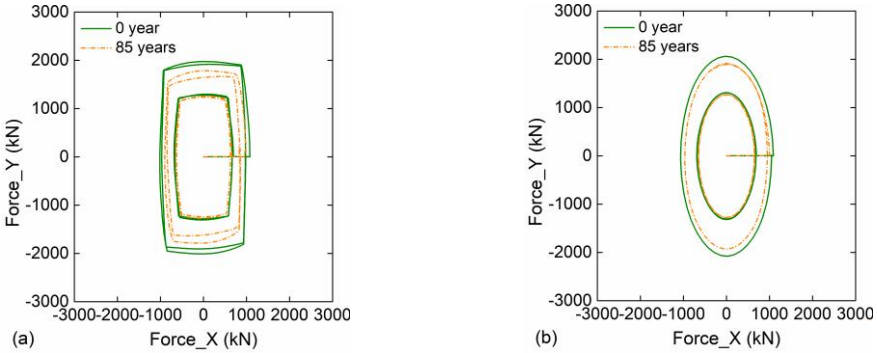


Figure 10. Biaxial force trajectories for the first two displacement amplitudes: (**a**) SS path; (**b**) CS path.

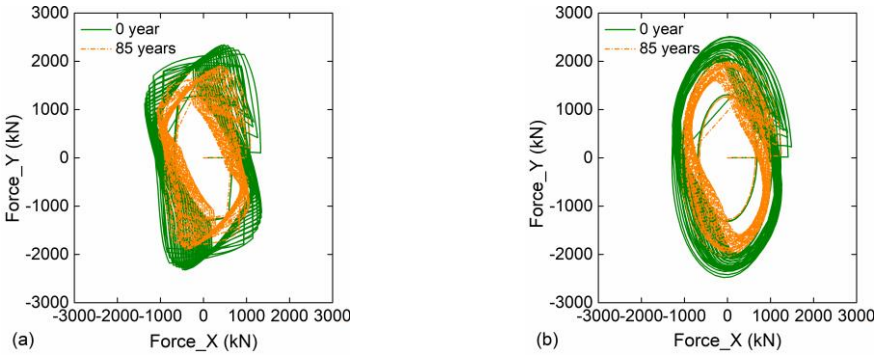


Figure 11. Biaxial force trajectories for all the displacement amplitudes: (**a**) SS path; (**b**) CS path.

4.6. Strength and Deformation Capacity

The skeleton curve of corroded piers in X- and Y-directions can be determined based on cyclic loops. The obtained skeleton curve at 0 years was selected and is presented in Figure 12. The uniaxial loading condition is also plotted in comparison. From Figure 12, it can be seen that the initial stiffness of the pier is almost the same for the uniaxial loading and biaxial loading conditions. After the yielding of the pier, the skeleton curve is influenced by the loading path. In both the X- and Y-directions of the pier, the peak force is reduced and the strength reduction trend increases as a result of the bilateral loading compared with the uniaxial loading condition. This is attributed to the strong coupling effect of the two-dimensional loading. From Figure 12, it can also be seen that the seismic performance in the X-direction is lower than that in the Y-direction. This is due to the fact that the X-direction is the weak-axis direction of the pier. Compared to the SS pattern, the deformation capacity for the CS pattern is smaller, especially in the X- direction. The peak force of the pier under the CS path is larger than that under the SS condition.

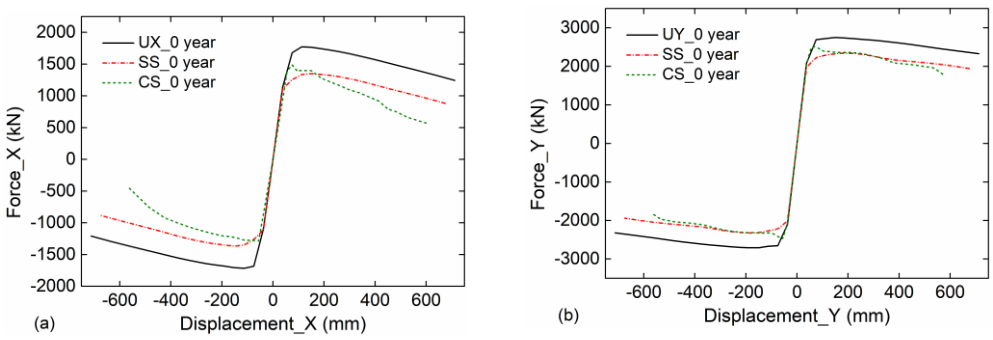


Figure 12. Skeleton curves of piers at 0 years: (**a**) X-direction; (**b**) Y-direction.

Not only load path but also corrosion level influence the seismic performance of the pier. To quantify this phenomenon, the time-dependent residual peak force, $F(t)$, and residual ultimate displacement, $D(t)$ (displacement corresponding to 85% of the peak force), of the pier is obtained based on the skeleton curve. Then, the normalized residual peak force (NRPF(t)) and normalized residual ultimate displacement (NRUD(t)) are calculated by Formulas (10) and (11).

$$NRPF(t) = \frac{F(t)}{F_U} \tag{10}$$

$$NRUD(t) = \frac{D(t)}{D_U} \tag{11}$$

where, F_U and D_U are the peak force and ultimate displacement of the pristine pier.

The NRPF(t) at both the X-direction and the Y-direction are compared in Figure 13. As shown in Figure 13a, for the UX loading condition, the peak force of the pier is slightly reduced from 1773 kN to 1762 kN during the time range of 0 years to 45 years. After 45 years, the NRPF drops with time from 0.99 to 0.81 due to the increase in corrosion damage. Compared with the UX pattern, the CS condition will lead to a more significant reduction of residual strength for the same level corroded pier. During the time range of 45 years to 85 years, the NRPF decreases from 0.83 to 0.65. Compared with the CS pattern, the coupling SS biaxial loading and corrosion has a more adverse effect on the loading carrying capacity of the in-service bridge pier. At 85 years, the NRPF for the SS path is 0.6, which is 5% and 21% smaller than that for the CS and UX conditions. The strength deterioration trend in the Y-direction is similar to that in the X-direction, as presented in Figure 13b. From Figure 13, it can also be seen that the peak force in the X-direction of the pier is smaller than that in the Y-direction. This phenomenon is due to the fact that the weak axis lies in the X-direction and the strong axis lies in the Y-direction. Based on the above analysis, it is confirmed that the coupling effect of corrosion and biaxial loading is detrimental to the load-bearing capacity of the rectangular pier. This problem for the pier under the SS loading path is more substantial than that under the CS loading path.

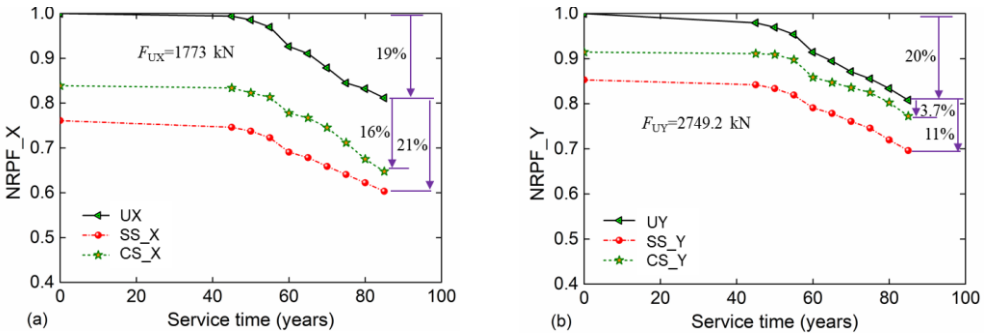


Figure 13. Time-dependent normalized residual peak force: (**a**) X-direction; (**b**) Y-direction.

Except for the peak strength, the deformation capacity of piers is also reduced as a result of corrosion damage and the biaxial loading coupling effect. This phenomenon is reflected by the time-variant NRUD, as shown in Figure 14. From Figure 14a, it can be seen that NRUD for the UX loading condition of the pier decreases from 1 to 0.72 over 85 years. Compared to the UX condition, the NRUD for the SS condition reduces from 0.91 to 0.71. The NRUD for the CS condition fluctuates in the range of 0.41 to 0.51, which is smaller than that for the UX and SS loading conditions. In the Y-direction, the decreasing trend of residual deformation capacity of the pier is observed for the three loading paths (Figure 14b). At 85 years, a reduction percentage of 5.3% and 39% for NRUD is observed under the SS and CS conditions compared with the UY condition. Figure 14 also shows that the ultimate displacement in the X-direction of the pier is different from that in the Y-direction. The reason for this phenomenon is because the pier section has a weak axis and a strong axis. From the above analysis, it is concluded that the coupling

effect of corrosion and biaxial loading on the deformation capacity of the rectangular pier is significant, especially for the CS loading pattern.

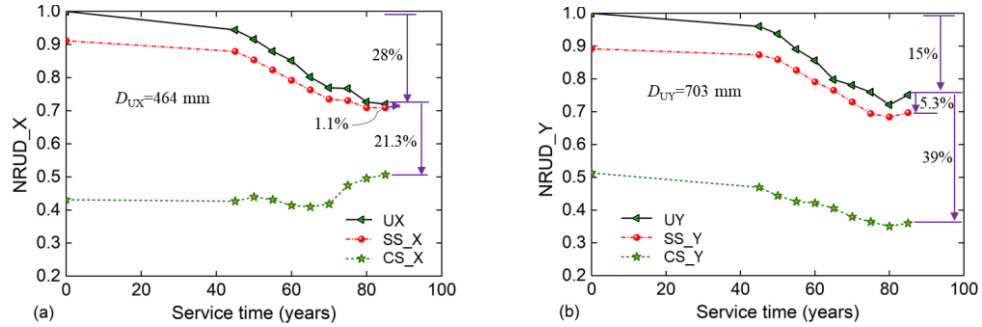


Figure 14. Time-dependent normalized residual ultimate displacement: (**a**) X-direction; (**b**) Y-direction.

4.7. Energy Dissipation Capacity

The energy dissipation capacity of the structure is decided by the enclosed area of the hysteretic curve. The cumulative dissipated energy for the pier under four loading paths at 0, 55, and 85 years are compared in Figure 15. From Figure 15, it can be seen that the dissipated energy is significantly influenced by the biaxial loading pattern for the same-level corroded piers. For the same corrosion degree, the dissipated energy under the UX path is the smallest among the four loading paths. Compared with the X-direction, the Y-direction is the strong axis direction. Therefore, the energy dissipation capacity in the Y-direction is larger than that in the X-direction. Due to the strong coupling effect and the energy dissipation in two directions, the pier under the CS pattern and SS pattern dissipated more energy than the uniaxial loading condition. Figure 15 also shows that the energy dissipation capacity is slightly reduced over 55 years. A sharp decrease in energy dissipation ability is found for 85 years compared with 55 years. This is attributed to the cross-sectional area reduction of reinforcement and deterioration of both the core concrete and the concrete cover. For example, at the maximum displacement amplitude of 712.5 mm, the energy of the pier under the UX pattern reduced from 46.4 $\times$ 10^3 kN. m to 38 $\times$ 10^3 kN. m, with a reduction percentage of 18.1%. The corresponding value for the pier at the maximum displacement under UY, CS, and SS patterns are 19.1%, 17.7%, and 18.3%, respectively.

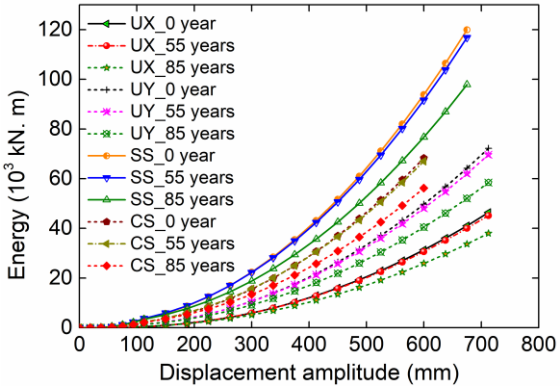


Figure 15. Cumulative dissipated energy for different displacement patterns and times.

5. Conclusions

This study explored the corrosion-induced time-dependent biaxial seismic performance of rectangular RC bridge piers. Based on the verified numerical model, the cyclic behavior of piers under different corrosion degrees and four loading paths is simulated and compared. The main conclusions based on the results are as follows:

(1) The hysteretic behavior of the rectangular bridge pier is significantly influenced by the trajectory of biaxial loading paths and the corrosion level. The seismic performance for both biaxial-loaded and uniaxial-loaded piers decreases slowly and then more quickly with the corrosion time.

(2) The loading path effect of biaxial loading for the arbitrarily corrosive pier includes two stages. In the elastic deformation stage, the trajectory of biaxial force for the pier under circular-shaped and square-shaped displacement patterns are elliptical and rectangular, respectively. In the plastic deformation stage, the biaxial force relationship presents a torsional rectangle and a torsional ellipse compared with the biaxial force trajectory of the elastic stage.

(3) The coupling effect of corrosion and biaxial loading is detrimental to the load-bearing capacity and deformation ability of the rectangular pier. For the pier with a corrosion level of 13.7% under the SS path, compared with the uniaxially loaded sound pier, there is a 40% and 31% reduction of peak strength in the X-direction and the Y-direction, respectively. The corrosion degree of 13.7% and CS loading path results in a 49.3% and 54% decrease in ultimate displacement for the pier in the X- and Y-directions compared to the uniaxial loaded uncorroded pier.

(4) For the same corrosion degree, the dissipated energy under the square-shaped biaxial displacement path is the biggest among the four loading paths, followed by the circular-shaped biaxial displacement path, strong-axis uniaxial displacement path, and weak-axis uniaxial displacement path.

Based on the results of this study, it is recommended to consider the coupling biaxial loading during the seismic assessment of the RC bridge pier located in a corrosive environment. It should be noted that this study uses the simple pitting corrosion models of the reinforcement. Both the uniform corrosion and pitting corrosion modeling should be incorporated; in addition, their deterioration effects on the mechanical properties of steel bars and concrete should be considered in a future numerical study. Furthermore, the seismic performance of corroded columns under more realistic and complex biaxial loading paths needs to be investigated in both experimental and computational works.

Author Contributions: Conceptualization, W.Y.; methodology, W.Y.; software, W.Y. and X.L.; investigation, formal analysis, X.L. and X.P.; supervision, W.Y.; writing—original draft preparation, W.Y.; writing—review and editing, X.P., C.T., Z.L., P.Z. and Y.W. All authors have read and agreed to the published version of the manuscript.

Funding: This research was funded by financial support from the Natural Science Foundation of Jiangsu Province (Grants No BK20210514) and the China Postdoctoral Science Foundation (Grants No 2020M681767).

Data Availability Statement: Not applicable.

Acknowledgments: The authors greatly appreciate the financial support from the Natural Science Foundation of Jiangsu Province (Grants No BK20210514) and the China Postdoctoral Science Foundation (Grants No 2020M681767).

Conflicts of Interest: The authors declare no conflict of interest.

References

1. Luo, Q.; Xu, G.; Zhao, J.; Wang, Q. Evolution characteristics of secondary tensile mechanical properties of corroded rebars. *Structures* **2021**, *34*, 3478–3486. [CrossRef]
2. Jin, L.; Li, Y.X.; Zhang, R.B.; Du, X.L. Mesoscopic investigation on seismic performance of corroded reinforced concrete columns. *Earthq. Eng. Eng. Vib.* **2022**, *21*, 969–985. [CrossRef]
3. Han, S.J.; Ju, H.; Lee, D. Practical approach for estimating flexural strengths of corroded RC members considering bond strength degradation. *Structures* **2022**, *39*, 808–820. [CrossRef]
4. Anania, L.; Badalà, A.; D'Agata, G. Damage and collapse mode of existing post tensioned precast concrete bridge: The case of Petrulla viaduct. *Eng. Struct.* **2018**, *162*, 226–244. [CrossRef]
5. Biswas, R.K.; Iwanami, M.; Chijiwa, N.; Nakayama, K. Structural assessment of the coupled influence of corrosion damage and seismic force on the cyclic behaviour of RC columns. *Constr. Build. Mater.* **2021**, *304*, 124706. [CrossRef]

6. Yuan, Z.J.; Fang, C.Q.; Parsaeimaram, M.; Yang, S. Cyclic Behavior of Corroded Reinforced Concrete Bridge Piers. *J. Bridge Eng.* **2017**, *22*, 04017020. [CrossRef]
7. Meda, A.; Mostosi, S.; Rinaldi, Z.; Riva, P. Experimental evaluation of the corrosion influence on the cyclic behaviour of RC columns. *Eng. Struct.* **2014**, *76*, 112–123. [CrossRef]
8. Li, D.W.; Wei, R.; Xing, F.; Sui, L.L.; Zhou, Y.W.; Wang, W.Y. Influence of Non-uniform corrosion of steel bars on the seismic behavior of reinforced concrete columns. *Constr. Build. Mater.* **2018**, *167*, 20–32. [CrossRef]
9. Dai, K.-Y.; Liu, C.; Lu, D.-G.; Yu, X.-H. Experimental investigation on seismic behavior of corroded RC columns under artificial climate environment and electrochemical chloride extraction: A comparative study. *Constr. Build. Mater.* **2020**, *242*, 118014. [CrossRef]
10. Guo, A.X.; Li, H.T.; Ba, X.; Guan, X.C.; Li, H. Experimental investigation on the cyclic performance of reinforced concrete piers with chloride-induced corrosion in marine environment. *Eng. Struct.* **2015**, *105*, 1–11. [CrossRef]
11. Yuan, W.; Guo, A.X.; Li, H. Experimental investigation on the cyclic behaviors of corroded coastal bridge piers with transfer of plastic hinge due to non-uniform corrosion. *Soil Dyn. Earthq. Eng.* **2017**, *102*, 112–123. [CrossRef]
12. Zhou, H.J.; Xu, Y.N.; Peng, Y.R.; Liang, X.B.; Li, D.W.; Xing, F. Partially corroded reinforced concrete piers under axial compression and cyclic loading: An experimental study. *Eng. Struct.* **2020**, *203*, 109880. [CrossRef]
13. Zhao, J.F.; Lin, Y.; Li, X.; Meng, Q.Y. Experimental study on the cyclic behavior of reinforced concrete bridge piers with non-uniform corrosion. *Structures* **2021**, *33*, 999–1006. [CrossRef]
14. Ma, Y.; Che, Y.; Gong, J.X. Behavior of corrosion damaged circular reinforced concrete columns under cyclic loading. *Constr. Build. Mater.* **2012**, *29*, 548–556. [CrossRef]
15. Rinaldi, Z.; Di Carlo, F.; Spagnuolo, S.; Meda, A. Influence of localised corrosion on the cyclic response of reinforced concrete columns. *Eng. Struct.* **2022**, *256*, 114037. [CrossRef]
16. Chinnasamy, Y.; Joanna, P.S.; Kothanda, K.; Gurupatham, B.G.A.; Roy, K. Behavior of Pultruded Glass-Fiber-Reinforced Polymer Beam-Columns Infilled with Engineered Cementitious Composites under Cyclic Loading. *J. Compos. Sci.* **2022**, *6*, 338. [CrossRef]
17. Kashani, M.M.; Lowes, L.N.; Crewe, A.J.; Alexander, N.A. Nonlinear fibre element modelling of RC bridge piers considering inelastic buckling of reinforcement. *Eng. Struct.* **2016**, *116*, 163–177. [CrossRef]
18. Cheng, H.; Li, H.N.; Biondini, F.; Wang, D.S.; Zou, Y. Strain penetration effect on cyclic response of corroded RC columns. *Eng. Struct.* **2021**, *243*, 112653. [CrossRef]
19. Xu, J.G.; Hong, W.; Zhang, J.; Hou, S.T.; Wu, G. Seismic performance assessment of corroded RC columns based on data-driven machine-learning approach. *Eng. Struct.* **2022**, *255*, 113936. [CrossRef]
20. El-Joukhadar, N.; Dameh, F.; Pantazopoulou, S. Seismic Modelling of Corroded Reinforced Concrete Columns. *Eng. Struct.* **2023**, *275*, 115251. [CrossRef]
21. Li, H.H.; Li, L.F.; Zhou, G.J.; Xu, L. Effects of various modeling uncertainty parameters on the seismic response and seismic fragility estimates of the aging highway bridges. *Bull. Earthq. Eng.* **2020**, *18*, 6337–6373. [CrossRef]
22. Li, H.H.; Li, L.F.; Zhou, G.J.; Xu, L. Time-dependent Seismic Fragility Assessment for Aging Highway Bridges Subject to Non-uniform Chloride-induced Corrosion. *J. Earthq. Eng.* **2020**, *26*, 3523–3553. [CrossRef]
23. Sengupta, A.; Quadery, L.; Sarkar, S.; Roy, R. Influence of Bidirectional Near-Fault Excitations on RC Bridge Piers. *J. Bridge Eng.* **2016**, *21*, 04016034. [CrossRef]
24. Qiu, F.W.; Li, W.F.; Pan, P.; Qian, J.R. Experimental tests on reinforced concrete columns under biaxial quasi-static loading. *Eng. Struct.* **2002**, *24*, 419–428. [CrossRef]
25. Tsuno, K.; Park, R. Experimental study of reinforced concrete bridge piers subjected to bi-directional quasi-static loading. *Doboku Gakkai Ronbunshu* **2004**, *752*, 11–26. [CrossRef] [PubMed]
26. Jia, J.; Zhang, K.; Wu, S.; Guo, Y.; Du, X.; Wang, X. Seismic performance of self-centering precast segmental bridge columns under different lateral loading directions. *Eng. Struct.* **2020**, *221*, 111037. [CrossRef]
27. Rodrigues, H.; Arêde, A.; Varum, H.; Costa, A.G. Experimental evaluation of rectangular reinforced concrete column behaviour under biaxial cyclic loading. *Earthq. Eng. Struct. Dyn.* **2013**, *42*, 239–259. [CrossRef]
28. Rodrigues, H.; Furtado, A.; Arêde, A. Experimental evaluation of energy dissipation and viscous damping of repaired and strengthened RC columns with CFRP jacketing under biaxial load. *Eng. Struct.* **2017**, *145*, 162–175. [CrossRef]
29. Li, C.; Hao, H.; Bi, K.M. Seismic performance of precast concrete-filled circular tube segmental column under biaxial lateral cyclic loadings. *Bull. Earthq. Eng.* **2019**, *17*, 271–296. [CrossRef]
30. Shirmohammadi, F.; Esmaeily, A. Performance of reinforced concrete columns under bi-axial lateral force/displacement and axial load. *Eng. Struct.* **2015**, *99*, 63–77. [CrossRef]
31. Al-Kaseasbeh, Q.; Mamaghani, I.H.P. Thin-Walled Steel Stiffened Square Box Columns with Uniform and Graded Thickness under Bidirectional Cyclic Loading. *Eng. Struct.* **2020**, *219*, 110919. [CrossRef]
32. Zheng, X.P.; Zhuo, W.D.; Wu, Z.Q.; Zhang, H.; Zhang, W. Quasi-static test of corroded RC bridge column under biaxial loading. *J. Fuzhou Univ. Nat. Sci. Ed.* **2016**, *44*, 516–523. (In Chinese)
33. Yuan, W.T.; Guo, A.X.; Yuan, W.; Li, H. Experimental investigation on cyclic behavior of coastal bridge piers with non-uniform corrosion under biaxial quasi-static loads. *Constr. Build. Mater.* **2018**, *190*, 222–234. [CrossRef]
34. Bhargava, K.; Mori, Y.; Ghosh, A.K. Time-dependent reliability of corrosion-affected RC beams. Part 3: Effect of corrosion initiation time and its variability on time-dependent failure probability. *Nucl. Eng. Des.* **2010**, *241*, 1395–1402. [CrossRef]

35. Vu, K.A.T.; Stewart, M.G. Structural reliability of concrete bridges including improved chloride-induced corrosion models. *Struct. Saf.* **2000**, *22*, 313–333. [CrossRef]
36. Duprat, F. Reliability of RC beams under chloride-ingress. *Constr. Build. Mater.* **2007**, *21*, 1605–1616. [CrossRef]
37. Stewart, M.G.; Wang, X.; Nguyen, M.N. Climate change impact and risks of concrete infrastructure deterioration. *Eng. Struct.* **2011**, *33*, 1326–1337. [CrossRef]
38. Val, D.V. Deterioration of Strength of RC Beams due to Corrosion and Its Influence on Beam Reliability. *J. Struct. Eng.* **2007**, *133*, 1297–1306. [CrossRef]
39. Yuan, W.T.; Fang, Q.H.; Dong, Z.X. Evaluation of Biaxial Strength Deterioration for Coastal Bridge Piers under Non-uniform Corrosion. *KSCE J. Civ. Eng.* **2021**, *26*, 1329–1343. [CrossRef]
40. Du, Y.G.; Clark, L.A.; Chan, A.H.C. Residual capacity of corroded reinforcing bars. *Mag. Concr. Res.* **2005**, *57*, 135–147. [CrossRef]
41. Finozzi, I.; Saetta, A.; Budelmann, H. Structural response of reinforcing bars affected by pitting corrosion: Experimental evaluation. *Constr. Build. Mater.* **2018**, *192*, 478–488. [CrossRef]
42. Shaikh, F.U.A. Effect of Cracking on Corrosion of Steel in Concrete. *Int. J. Concr. Struct. Mater.* **2018**, *12*, 3. [CrossRef]
43. Coronelli, D.; Gambarova, P. Structural Assessment of Corroded Reinforced Concrete Beams: Modeling Guidelines. *J. Struct. Eng.* **2004**, *130*, 1214–1224. [CrossRef]
44. Biondini, F.; Vergani, M. Damage modeling and nonlinear analysis of concrete bridges under corrosion. In *Proceedings of the Sixth International Conference of Bridge Maintenance, Safety and Management (IABMAS 2012), Lake Maggiore, Italy, 8–12 July 2012*; CRC Press/Balkema, Taylor and Francis Group: Boca Raton, FL, USA, 2012; pp. 949–957.
45. Branco, R.; Costa, J.D.; Berto, F.; Kotousov, A.; Antunes, F.V. Fatigue crack initiation behaviour of notched 34CrNiMo6 steel bars under proportional bending-torsion loading. *Int. J. Fatigue* **2020**, *130*, 105268. [CrossRef]
46. Luo, P.; Yao, W.; Susmel, L.; Li, P. Prediction of fatigue damage region with the use of the notch critical plane approach for crack initiation and propagation. *Int. J. Fatigue* **2020**, *135*, 105533. [CrossRef]
47. Mander, J.; Priestley, M. Theoretical Stress-Strain model for confined concrete. *J. Struct. Eng.* **1988**, *114*, 1804–1826. [CrossRef]
48. Mazzoni, S.; McKenna, F.; Scott, M.H.; Fenves, G.L. *OpenSees Command Language Manual*; Pacific Earthquake Engineering Research (PEER) Center: Berkeley, CA, USA, 2006.
49. Mangalathu, S.; Soleimani, F.; Jeon, J.-S. Bridge classes for regional seismic risk assessment: Improving HAZUS models. *Eng. Struct.* **2017**, *148*, 755–766. [CrossRef]

Disclaimer/Publisher's Note: The statements, opinions and data contained in all publications are solely those of the individual author(s) and contributor(s) and not of MDPI and/or the editor(s). MDPI and/or the editor(s) disclaim responsibility for any injury to people or property resulting from any ideas, methods, instructions or products referred to in the content.